JOURNAL OF MATERIALS SCIENCE 13 (1978) 1187–1194

Plastic instability related to grain-boundary failure in an Al-Zn-Mg alloy at low temperatures

MUTSUMI ABE, AKIRA FUJIWARA
Central Research Laboratory, Kobe Steel Ltd., Kobe, Japan

The strength and ductility of an Al–6 wt % Zn–1.2 wt % Mg alloy at low temperatures have been investigated by varying the grain size, the amount of grain-boundary precipitate and the nature of the precipitates in the matrix. Pronounced grain-boundary embrittlement has been observed at temperatures below −100° C in alloys age-hardened by GP zones and especially in coarse-grained alloy specimens, but was not observed in over-aged specimens. From the condition for plastic instability related to the grain-boundary micro-cracking, the temperature and structure dependences of the ultimate tensile properties are expressed by;

$$(\sigma_i - \sigma_0)/\sigma_i = \epsilon_u/n + C,$$

where σ_i is the instability stress (true ultimate tensile strength), σ_0 the 0.2% proof stress, ϵ_u the uniform elongation, n a constant found to be about $\frac{1}{2}$ and C a constant related to the work-hardening rate of the matrix.

1. Introduction

From studies on the mechanical properties of aluminium alloys at cryogenic temperatures [1, 2], it is known that the strength of pure aluminium increases with decreasing testing temperature [3] whereas the elongation or the reduction of area at low temperatures is much reduced due to grain-boundary embrittlement [4]. The tensile properties of age-hardened aluminium alloys at low temperatures, however, have not been systematically examined in relation to the structural factors such as grain size, the amount of grain-boundary precipitate and the nature of the precipitates in the matrix.

The present work aims at clarifying the relation between the above structural factors and properties such as the ultimate tensile strength and the uniform elongation in an Al–Zn–Mg alloy at low temperatures.

2. Experimental procedure

The Al–Zn–Mg alloy used in this investigation was prepared from high purity materials by semi-continuous casting in a mould 110 mm × 180 mm × 400 mm. The alloy compositions were 6.20 wt % Zn, 1.20 wt % Mg, 0.006 wt % Fe and 0.005 wt % Si. The cast ingot was homogenized at 450° C, scalped, and hot-rolled to 15 mm thickness. Tensile specimens having effective gauge measurements of 25 mm × 7 mm ϕ were milled from the strip. The solution heat-treatment was carried out at 450° C in air for 30 min, unless otherwise noted. The grain size was controlled by annealing at 500° C for various periods, and subsequently the specimens were solution heat-treated at 400° C for 10 min in a salt bath. Ageing treatments employed in this work were as follows;

Heat treatment A:

500° C (t) → 400° C for 10 min → water quenched

→ room temperature for 1 week → 70° C for 1 day

With this heat treatment, specimens with controlled grain sizes are age-hardened by GP zones.

Heat treatment B:

450° C for 30 min → 200° C (t) → water quenched

→ room temperature for 1 week → 70° C for 1 day

The amount of grain-boundary precipitate is controlled by varying the quench-interruption period at 200° C subsequent to the heat treatment at 450° C.

Heat treatment C:

500° C (t) → 400° C for 10 min → water quenched

→ 180° C for 1 day

Over-aged specimens having various grain sizes are obtained by this heat treatment.

After these treatments, tensile tests were made on an Instron-type machine at a strain rate 2.0×10^{-2} min^{-1} at room temperature (air), −40° C (methanol), −100° C (Difron), −150° C (Difron-12) and −196° C (liquid nitrogen). After the tensile test, the fractographic examination was performed by a scanning electron microscope.

3. Experimental results

3.1. Heat treatment A

Fig. 1 shows the temperature dependence of tensile properties such as 0.2% proof stress, σ_0, and engineering ultimate tensile strength, σ_b, for specimens containing GP zones in the matrix, as a function of grain size. As is seen from Fig. 1, the temperature dependence of σ_b varies with grain size; at temperatures below −100° C for the coarse grain size σ_b is much reduced. Fig. 2 shows the temperature dependence of the uniform elongation, δ_u, the elongation at the onset of necking, and also of the local elongation, δ_l the apparent elongation from maximum load to fracture. It is found that δ_u shows a maximum at about −100° C and also that δ_u for the coarse grain size become small at low temperatures as is the case of the engineering ultimate tensile strength. In order to illustrate the low temperature embrittlement, the temperature dependence of the instability stress, σ_i, the true stress at the onset of necking, is shown in Fig. 3 as a function of grain size. It can clearly be seen from Fig. 3 that the transition from ductile to brittle fracture occurs at temperatures between −100 and −150° C. It is also found from the fractographic examination that the apparent ratio of the inter-granular fracture region [5] increases with decreasing test temperature and with increasing grain size.

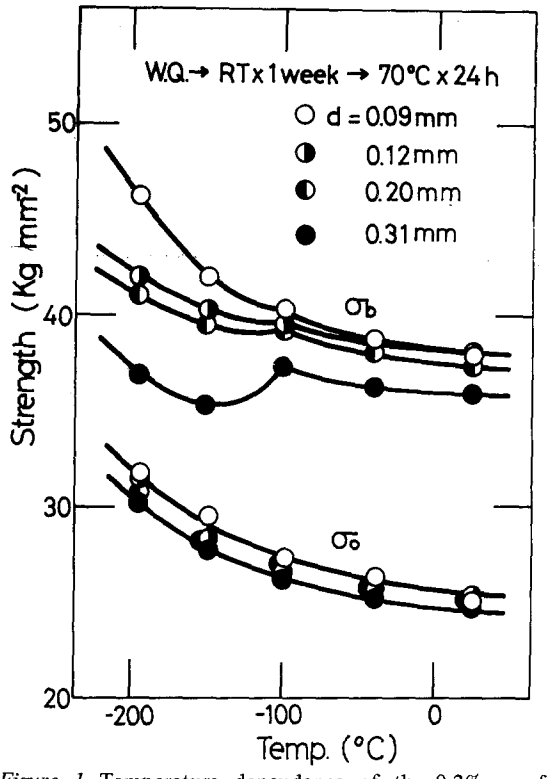

Figure 1 Temperature dependence of the 0.2% proof stress, σ_0, and the ultimate tensile strength, σ_b, as a function of grain size (heat treatment A).

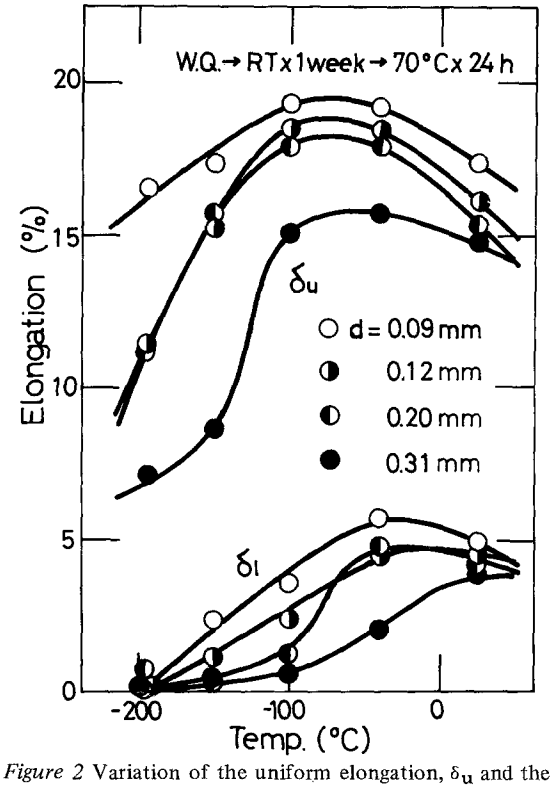

Figure 2 Variation of the uniform elongation, δ_u and the local elongation, δ_l, with the testing temperature in heat treatment A.

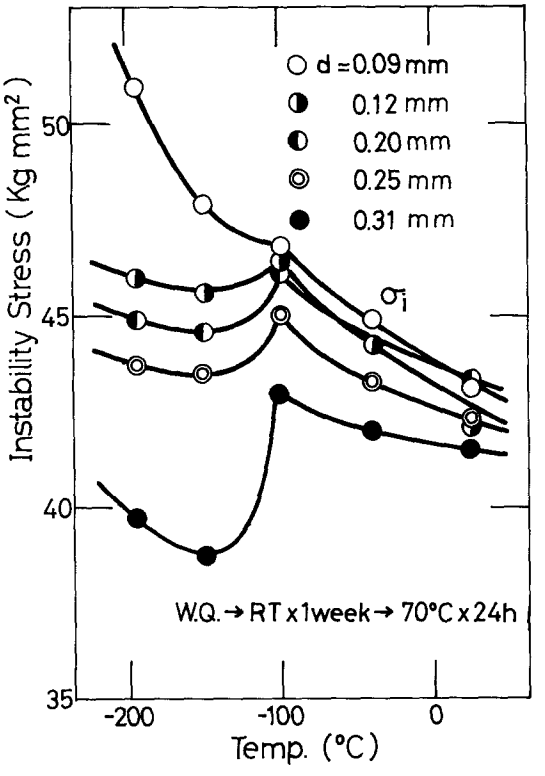

Figure 3 Effect of grain size on the temperature dependence of the instability stress, σ_i, obtained from Figs. 1 and 2. Note the drastic change of σ_i at -150° C in the coarse-grained specimen.

3.2. Heat treatment B

As was previously pointed out [6], the amount of grain-boundary precipitate (GBP) increases as the holding time at the quench-interruption temperature (200° C) is increased. With increased holding time at 200° C, the precipitate-free zone (PFZ) usually becomes wide. In order to eliminate the effect of the PFZ width, the specimens were subjected to the low-temperature ageing at both room temperature and 70° C, i.e., heat treatment B, by which the PFZ becomes very narrow, as pointed out by Cornish *et al.* [7]. Fig. 4 shows the temperature dependence of σ_0 and σ_b as functions of the quench-interruption period at 200° C in specimens having a coarse grain size. It is seen that the engineering ultimate tensile strength σ_b varies with the interruption period. The effect of the testing temperature on σ_b is not discontinuous; quite different from that for specimens subjected to heat treatment A (Fig. 1). The ultimate tensile strength increases smoothly at lower temperatures.

Fig. 5 shows the temperature variation of the uniform elongation, δ_u, and the local elongation, δ_l, with the amount of GBP for the same specimens as in Fig. 4. In comparison with Fig. 2, it is seen that δ_u does not show a maximum but de-

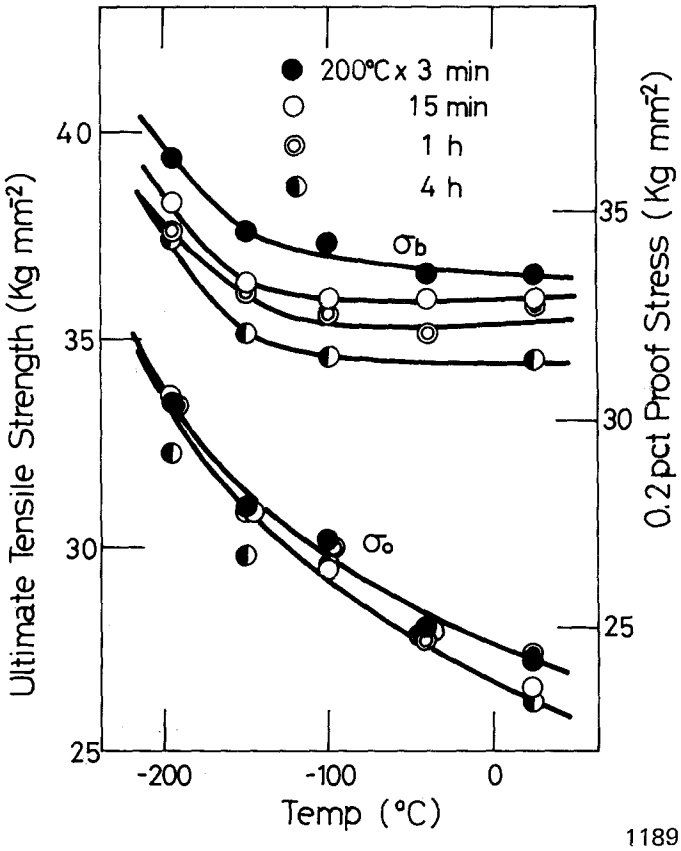

Figure 4 Temperature dependence of σ_0 and σ_b as functions of the amount of grain-boundary precipitate (quench-interruption periods) in heat treatment B.

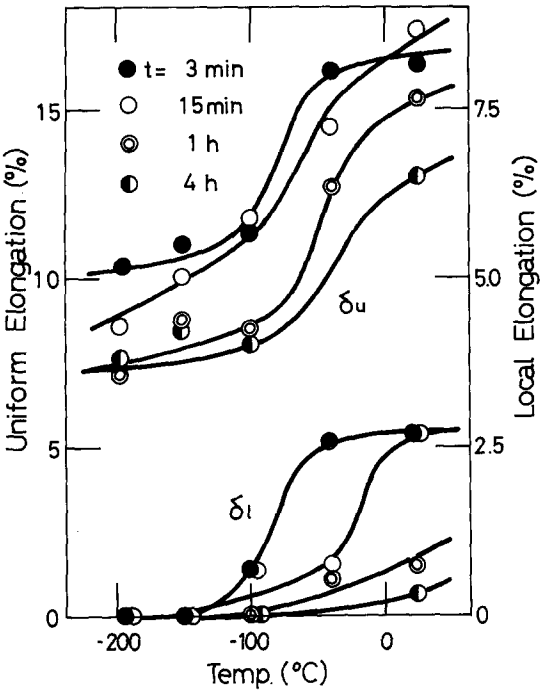

Figure 5 Variation of the elongations, δ_u and δ_l, with the experimental temperature (heat treatment B).

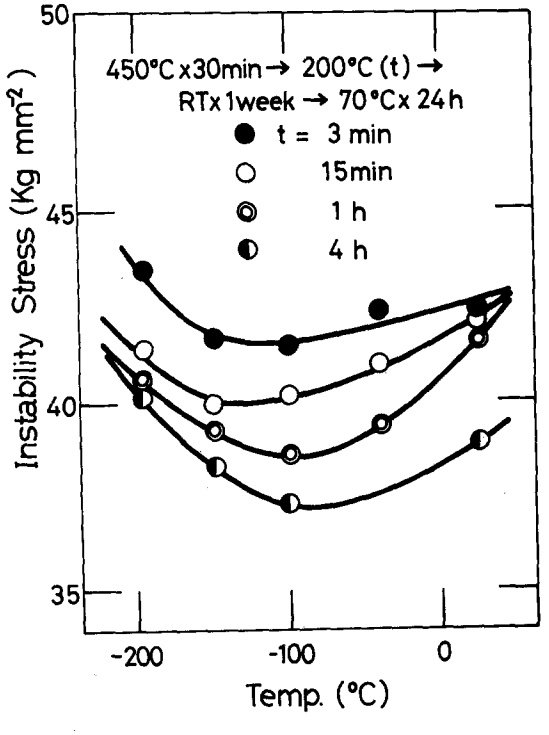

Figure 6 Effect of the quench-interruption period (the amount of grain-boundary precipitate) on the temperature dependence of the instability stress. Note the difference from Fig. 3.

creases with decreasing temperatures and with increasing amount of GBP. From the ultimate tensile properties such as σ_b and δ_u shown in Figs. 4 and 5, the temperature dependence of the instability stress is determined (Fig. 6).

3.3. Heat treatment C

The temperature variation of tensile properties with grain size in specimens containing over-aged precipitates is shown in Figs. 7 and 8. It is seen from Fig. 7 that the strength σ_b or σ_i increases steeply but monotonically with decreasing temperature, while the temperature variation of σ_0 is very small compared with that of the alloy age-hardened by GP zones (see Fig. 1). The grain size dependence of σ_b also is very small at the temperatures studied. It can also be noted from Fig. 8 that the uniform elongation δ_u increases with decreasing temperature whereas the local elongation δ_l shows a minimum corresponding to the plateau of the δ_u curve. Unlike for the previous heat treatments, the strengths σ_b and σ_i and the uniform elongation δ_u increase rather smoothly with decreasing temperature. However, the intergranular fracture at the fractured surface increases with decreasing testing temperature, and with increasing grain size, as in cases A and B.

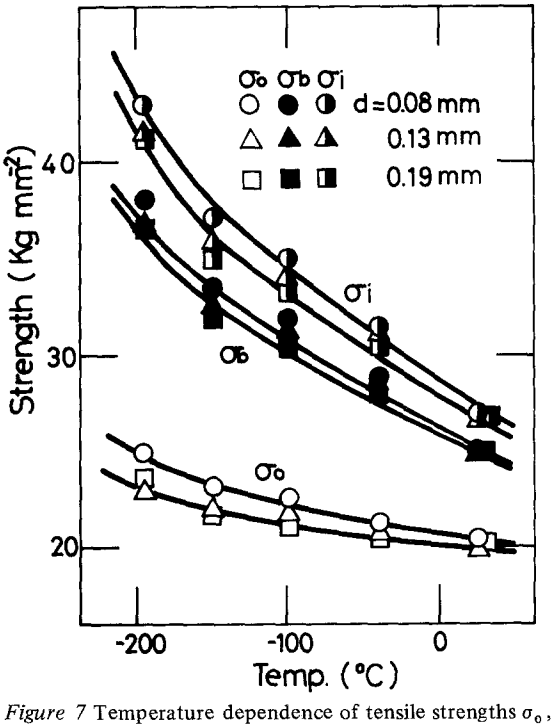

Figure 7 Temperature dependence of tensile strengths σ_0, σ_b and σ_i, as functions of the grain size in heat treatment C.

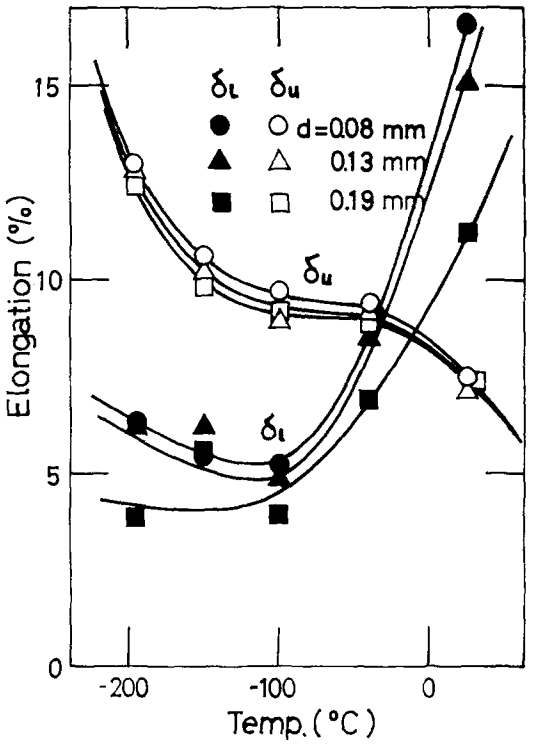

Figure 8 Variation of δ_u and δ_l with the testing temperature in heat treatment C. Note the increase of δ_u with decreasing temperature.

4. Discussion

4.1. Plastic instability and grain-boundary embrittlement

As was shown in the previous section, the uniform elongation in alloys age-hardened by GP zones (heat treatment A) decreases markedly at temperatures below $-100°$ C (Figs. 2 and 5), at which the ultimate tensile strength shows anomalous behaviour (Fig. 1) owing to grain-boundary fracture. On the other hand, when the matrix is over-aged (heat treatment C), the ultimate tensile strength as well as the uniform elongation increase monotonically at low temperatures, in spite of the similar grain-boundary fracture (Figs. 7 and 8). It seems that the ultimate tensile properties are affected not only by structural factors such as grain size, the nature of precipitates in the matrix, and the amount of GBP, but also by the susceptibility to grain-boundary fracture.

Fig. 9 shows the grain-boundary cracks observed in a specimen subjected to heat treatment A and deformed by about 10% at $-150°$ C. It is seen that grain-boundary cracking occurred prior to the maximum load in the load–deformation curve. Such behaviour is also observed in over-aged specimens. In the presence of grain-boundary micro-

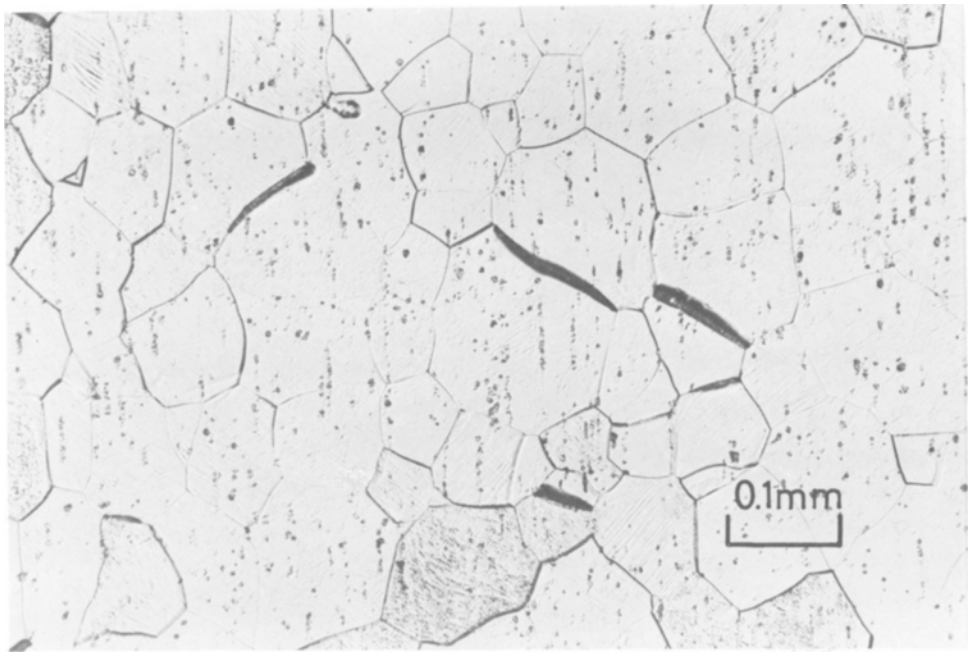

Figure 9 Grain-boundary micro-cracks observed in the specimen before reaching the maximum load (about 10% elongation) in heat treatment A at $-150°$ C.

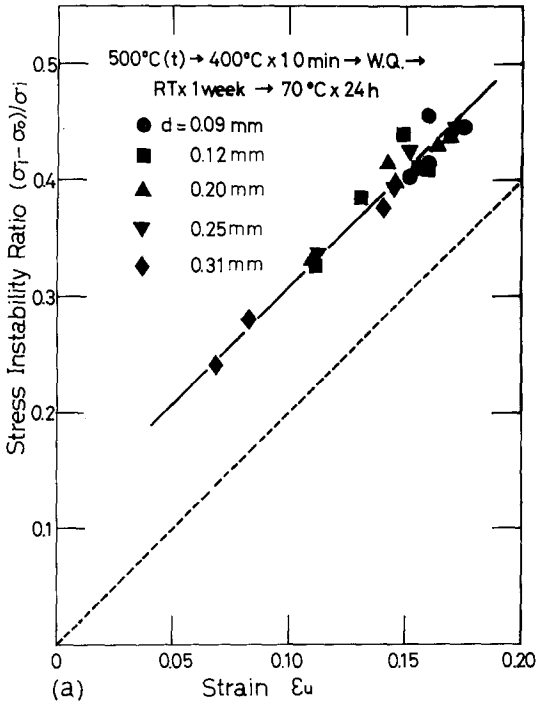

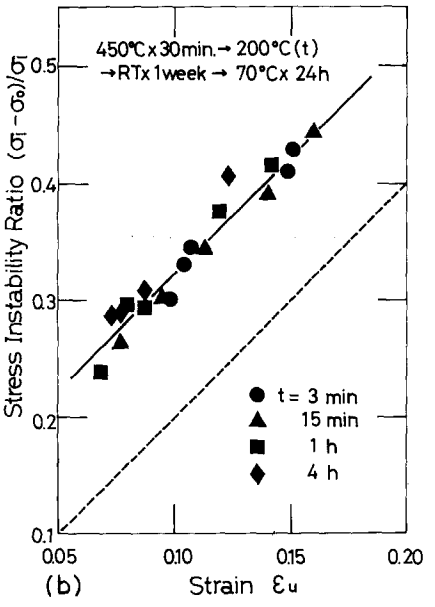

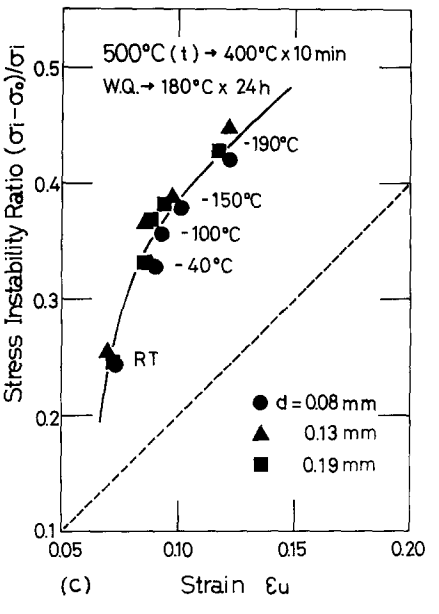

Figure 10 The relationship between σ_0, σ_i and ϵ_u expected from Equation 5 for heat treatments (a) A, (b) B, and (c) C, respectively.

cracks, the rate of reduction of the effective cross-sectional area bearing the load is expressed by the following equation;

$$dA/A = (dA/A)_p + (dA/A)_v, \qquad (1)$$

where $(dA/A)_p$ shows the reduction rate of the cross-sectional area caused by the plastic deformation, while $(dA/A)_v$ is the reduction rate owing to the growth of cavities within the cross-sectional plane. Here, the effective cross-sectional area does not mean the whole cross-sectional area of the specimen but shows the cross-sectional area actually bearing the load, and is smaller by the area covered with cavities. As is seen in Fig. 9, the grain-boundary micro-cracks show almost the same disk-like shape.

If the length of these disk-like cracks is restricted to the dimensions of the grain, the thickness must increase with increasing strain. Therefore, the area of cavities within the cross-sectional plane of the specimen increases with strain. Following Ashby [8], the area of cavities within the cross-sectional plane increases approximately in proportion to the strain, i.e., $(dA/A)_v = -q(dL/L)$, where q is the growth rate of micro-crack within the cross-sectional plane and dL/L is the strain of the specimen. Thus, Equation 1 may be rewritten as follows;

$$dA/A = -(1+q)dL/L. \qquad (2)$$

When the grain-boundary micro-cracking occurred prior to the maximum load, the necking condition may be obtained from Equation 2 as;

$$d\sigma/d\epsilon = (1+q)\sigma, \qquad (3)$$

instead of $d\sigma/d\epsilon = \sigma$ for the case of no micro-cracking, where σ is the true stress and ϵ the true strain. If the conventional relationship between stress and strain for the specimen containing

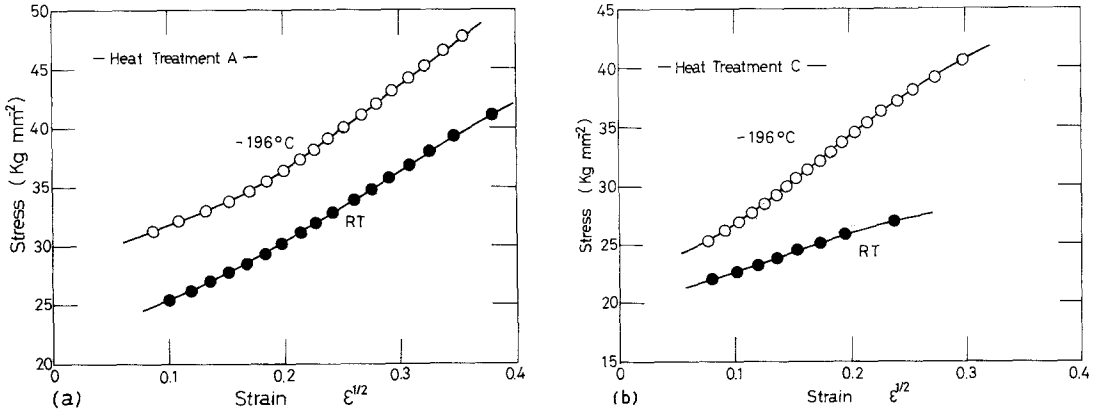

Figure 11 Stress–strain curves at room temperature and −196° C for (a) heat treatment A, and (b) heat treatment C.

micro-cracks is represented by;

$$\sigma = \sigma_0 + K\epsilon^n, \tag{4}$$

where σ_0 is the 0.2% proof stress or the yield stress, and K and n are constants, a relationship at the onset of necking can be obtained from Equations 3 and 4 as;

$$(\sigma_i - \sigma_0)/\sigma_i = (1+q)\epsilon_u/n. \tag{5}$$

The plots of the experimental data using Equation 5 for specimens subjected to heat treatments A, B and C are shown in Figs. 10a to c, respectively. The dotted lines in these figures represents the relation expected from Equation 5 when the constant n is assumed to be $\frac{1}{2}$ and the growth rate q to be 0. Thus, the experimental data may be represented by the following equation;

$$(\sigma_i - \sigma_0)/\sigma_i = \epsilon_u/n + C, \tag{6}$$

where n is nearly constant at $\frac{1}{2}$, and C is a constant independent of the testing temperature for heat treatments A and B (Figs. 10a and b). For heat treatment C (Fig. 10c), however, C is not constant and depends upon the testing temperature. It is thus considered that the constant C is related to the nature of the precipitates in the matrix.

From comparison of Equations 5 and 6, it is seen that $q\epsilon/n \simeq C$, i.e., the micro-cracked area $q\epsilon$ in Equation 5 becomes constant at the onset of necking when the matrix is age-hardened by GP zones (heat treatments A and B). In other words, the necking occurs when the micro-cracked area ($q\epsilon_u$) within the cross-sectional area of specimen reaches the critical value, which is almost constant for alloys age-hardened by GP zones irrespective of the testing temperature, grain size and the amount of GBP. On the other hand, for the over-aged alloy (heat treatment C), the critical cracked area varies with the testing temperature but not with grain size (Fig. 10c). The difference in the critical cracked areas based on the nature of the precipitate in the matrix is considered to be related to the temperature dependence of the strain-hardening capacity in the region surrounding the micro-crack [9]. In order to verify the influence of the nature of the matrix precipitate on the critical cracked area, the stress–strain curves at room temperature and −196° C for specimens subjected to heat treatments A and C are compared, as shown in Figs. 11a and b, respectively. In these figures, the strain is represented by its square root. As is seen from these figures, for heat treatment A, the slope of the curves $K(=\mathrm{d}\sigma/\mathrm{d}\sqrt{\epsilon})$ is not much affected by the testing temperature, while for heat treatment C the slope increases markedly as the temperature is lowered, enough to suggest that the strain-hardening capacity is much affected by the testing temperature in the over-aged alloy (heat treatment C).

4.2. Ultimate tensile properties

Since the linear relationship given by Equation 6 was obtained at the onset of necking for heat treatments A and B (age-hardened by GP zones), the true ultimate tensile stress σ_i and the uniform elongation ϵ_u can be given from Equations 3, 4 and 5, by assuming the constant n to be $\frac{1}{2}$ (obtained from Figs. 10a and b), as;

$$\sigma_i = \sigma_0/2 + \sqrt{[\sigma_0^2 + 2K^2/(1+q)]}/2 \tag{7}$$

$$\epsilon_u = (1+q)^{-1} \times \left(\tfrac{1}{2} - 1/\{1 + \sqrt{[1 + 2K^2/(1+q)\sigma_0^2]}\}\right) \tag{8}$$

From Equations 7 and 8, it is seen that the stress and the strain at the maximum load are represented by the 0.2% proof stress, σ_0, the work hardening coefficient, K, and the growth rate of micro-cracking, q. It is also understood that the ultimate tensile stress, σ_i, and the uniform elongation, ϵ_u, decrease with increasing q. It is clear that the anomalous behaviour of σ_i at low temperatures shown in Fig. 3 can not be explained if $q = 0$.

The low temperature embrittlement shown in Fig. 3 is ascribable to the increase in the growth rate of micro-cracks, q, since σ_0 and K do not increase at low temperatures. In fact, ϵ_u decreases at low temperatures for heat treatment A and $q\epsilon_u$ is constant at the onset of necking, so that q must increase at low temperatures. Similarly, the influences of the grain size and the amount of GBP on the plastic instability (Figs. 2 and 5) can be explained in terms of the condition $q\epsilon_u$ being constant; the growth rate q increases with increasing grain size and the amount of GBP. On the other hand, in over-aged specimens (heat treatment C), the temperature dependence of the work-hardening coefficient K is responsible for the tensile properties such as σ_i and ϵ_u, rather than the growth rate q, for the growth rate decreases at low temperatures (Fig. 10c).

5. Summary

Tensile properties of an Al–6 wt % Zn–1.2 wt % Mg alloy at low temperatures have been investigated with particular reference to the plastic instability caused by the grain-boundary micro-cracking. The results obtained are summarized as follows.

(1) Anomalous grain-boundary embrittlement was observed at temperatures below -100° C in the alloy age-hardened by GP zones (heat treatments A and B), especially in specimens with coarser grains.

(2) When the matrix is over-aged (heat treatment C), the ultimate tensile strength and the uniform elongation increase with decreasing test temperature regardless of the grain size, while the local elongation decreases.

(3) A linear relationship between 0.2% proof stress, σ_0, true ultimate tensile strength, σ_i, and uniform elongation, ϵ_u, was obtained as

$$(\sigma_i - \sigma_0)/\sigma_i = \epsilon_u/n + C,$$

where the constant $n = \frac{1}{2}$ and the constant C depends on the work-hardening rate in the matrix. This relationship holds independently of the deformation temperature, grain size, amount of GBP (grain-boundary precipitates) and the nature of the precipitate in the matrix.

(4) The anomalous behaviour at low temperatures has been interpreted from the analysis based on the above relationship, with reference to the growth rate of the grain-boundary micro-cracks.

Acknowledgements

The authors wish to thank Professor J. Takamura, Kyoto University, for his helpful discussions and suggestions during the course of this investigation. The paper is published by permission of Kobe Steel, Ltd.

References

1. J. G. KAUFMAN, K. O. BOGARDUS and E. T. WANDERER, *Advances in Cryogenic Eng.* **13** (1967) 294.
2. J. D. EMBURY and E. NES, *Z. Metallkde* **65** (1974) 45.
3. R. P. CARREKER Jr and W. R. HIBBARD Jr, *J. Metals* 9 (1957) 1157.
4. G. Y. CHIN, W. F. HOSFORD Jr and W. A. BACKOFEN, *Trans. Met Soc. AIME* **230** (1964) 437.
5. B. B. RATH and I. M. BERNSTEIN, *Met. Trans.* **2** (1971) 2845.
6. M. ABE, K. ASANO and A. FUJIWARA, *ibid* **4** (1973) 1499.
7. A. J. CORNISH and Miss M. K. B. DAY, *J. Inst. Metals* **97** (1969) 44.
8. M. F. ASHBY, *Phil. Mag.* **14** (1966) 1157.
9. G. T. HAHN and A. R. ROSENFIELD, *Met. Trans.* **6A** (1975) 653.

Received 19 July and accepted 16 September 1977.